Impact of Frequency Estimation for VSC-based Devices with Primary Frequency Control

Álvaro Ortega, *Member, IEEE*, Federico Milano, *Fellow, IEEE*
School of Electrical and Electronic Engineering
University College Dublin, Ireland

***Abstract*— This paper presents a comparison of the performance of frequency control devices considering different techniques to estimate the frequency deviation signal. We consider three estimation techniques, namely the center of inertia (COI), the frequency divider (FD) formula, and the phase-locked loop (PLL). The first two are based on the measurement of synchronous machine rotor angles and are virtually exact measures, while the latter is based on an electronic device and is affected by noise and numerical errors. The goal of the paper is first to define whether the PLL estimation is closer to the COI or to the FD. Then, the dynamic response of VSC-based wind power plants and energy storage systems providing primary frequency regulation is studied and compared using the three aforementioned signals. A comprehensive set of scenarios based on the WSCC 9-bus test system is presented in the case study.**

I. Introduction

Traditionally, synchronous machines were the main devices apt to provide primary frequency regulation in ac transmission grids. This situation is rapidly changing due to the increasing penetration of distributed, non-synchronous generation based on Renewable Energy Sources (RESs), such as wind and photo-voltaic power plants, as well as other emerging devices, such as Energy Storage Systems (ESSs). These devices, which generally are connected to the grid through Voltage Sourced Converters (VSCs), reduce the overall system inertia and increase the risk of frequency and voltage instabilities. This fact has led, in recent years, to the development of a large variety of frequency regulation strategies for RESs [1]–[3].

In practice, the frequency regulated by RESs and ESSs is measured locally through Phase-Locked Loop (PLL) devices. Such electronic devices are crucial for the proper synchronization and regulation of VSCs and several implementations exist (see, for example, [4] for a comprehensive survey on different PLL solutions). From a simulation point of view, however, the frequency control through VSC devices poses the problem of properly defining the frequency signal to be used as input of the regulators. While fully-fledged electromagnetic models are still impractical to simulate large power systems, conventional electro-mechanical models for transient stability analysis neglect *a priori* frequency variations in transmission lines and loads.

It has to be expected that, depending on the frequency estimation technique considered, different signals are originated, and therefore different responses are expected from frequency control devices. In [5], the authors have compared the response of thermostatically controlled loads that regulate the frequency locally by means of varying their reference temperature when their input signal is provided by different estimation approaches. However, the impact of PLL-based frequency estimation for RESs and ESSs that provide primary frequency regulation has not been studied yet.

This paper aims to fill this gap and provides two contributions, as follows.

- Definition of a model of PLL device that is adequate for conventional transient stability analysis of power systems based on lumped transmission line models and bus voltage phasors.
- Evaluation of the impact of PLL-based measured frequency deviations for the control of VSC-based renewable sources and ESSs.

With this aim, the paper compares the estimated frequency measured through the PLL with ideal signals, namely the Center of Inertia (COI) [6] and the Frequency Divider formula (FD) [7]. The latter was recently proposed by the authors and is an efficient and numerically stable alternative to the well-known washout filter [8].

The paper is organized as follows. The PLL model is provided in Section II. This section also briefly recalls the frequency estimation techniques based on the COI and the FD. The primary frequency control schemes of Wind Energy Conversion Systems (WECSs) and ESSs are presented in Sections III-A and III-B respectively. Section IV presents the case study based on the WSCC 9-bus test system. Finally, conclusions are drawn in Section V.

II. Frequency Estimation Techniques

This section presents a model of PLLs devices suitable for transient stability analysis and outlines theoretical frequency estimation models, namely the COI, and the FD formula.

A. Phase-Locked Loop

VSCs are synchronized to the grid by mean of PLLs. These are electronic circuits that consist of three main parts: (i) a phase detector (PD); (ii) a loop filter (LF); and (iii) and a voltage oscillator control (VOC). The PD measures abc voltages and convert them into $\alpha\beta$- and dq-reference frames while the VOC imposes that the v_q component is zero. There are many different implementations of the loop filter (see, for example, [4], [9], [10]) but, most commonly, it consists of a PI controller. An interesting by-product of any PLL is that the output of the

LF is an estimation of the frequency deviation at the bus of connection.

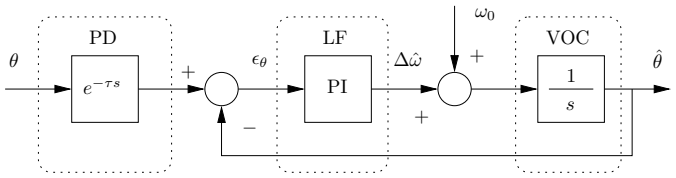

Fig. 1: Scheme of a synchronous reference frame PLL suitable for transient stability analysis.

A fundamental-frequency model of the PLL is proposed in Fig. 1. This implements a typical synchronous reference frame PLL where the PD is modeled as a pure delay; the LF is a PI controller; and the VOC is implemented as an integrator. The delay τ accounts for the time needed to: (i) retrieve the measures of the three-phase quantities from the grid; (ii) process the measures in order to obtain their dq-components; and (iii) compute the bus voltage phase angles and later the bus frequency signal.

The input of the PLL is the phase angle θ of the bus voltage phasor at which the PLL is connected and the output is the estimated phase angle $\hat{\theta}$. This representation is adequate if the voltage phasors are expressed in polar coordinates and are equivalent to tracking the v_q voltage component in rectangular coordinates. In fact, one has that $v_q = v \sin\theta$ and, thus, $v_q = 0$ implies $\theta = 0$.

Figure 1 also shows that the output of the PI controller is an estimation of the frequency deviations $\Delta\hat{\omega}$. The bus frequency estimation is thus given by $\omega_0 + \Delta\hat{\omega}$, where ω_0 is the synchronous speed. Since the input quantity θ is an algebraic variable in the standard transient stability model, the PLL can show numerical issues and provide a frequency estimation affected by jumps and discontinuities following discrete events in the system such as faults or line outages.

B. Center of Inertia and Frequency Divider

The COI has been widely utilized to estimate the average frequency of transmission systems, due mainly to its simple computation, which only requires the inertia constants and rotor speeds of the synchronous machines of the system, and its reasonable accuracy. Assuming that a set $\mathcal{G}$ of synchronous generators is connected to a given system, the COI can be computed as follows:

$$\omega_{\text{COI}} = \frac{\sum_{j\in\mathcal{G}} H_j \omega_j}{\sum_{j\in\mathcal{G}} H_j} \tag{1}$$

where ω_j are rotor speeds and H_j are inertia constants.

While the COI is a good candidate to represent inter-area oscillations among machine clusters and the overall trend of the system frequency, local frequency variations of the synchronous machines, and in particular of those with small inertia, cannot be captured.

An alternative approach to the COI to estimate local frequency variations has been recently proposed in [7]. The main hypothesis behind this approach, called by the authors as *frequency divider* (FD), is that the frequency varies as in a *continuum matter* along the impedances of the transmission lines, where the boundary conditions are defined by the synchronous machines operating in the system.

The interested reader can find the complete set of hypothesis and the detailed mathematical derivation of the FD formula in [7]. For clarity, however, the expression the FD formula is:

$$\mathbf{0} = (\mathbf{B}_{BB} + \mathbf{B}_{G0}) \cdot (\boldsymbol{\omega}_B - \mathbf{1}) + \mathbf{B}_{BG} \cdot (\boldsymbol{\omega}_G - \mathbf{1}) \tag{2}$$

where $\boldsymbol{\omega}_G$ are machine rotor speeds; $\boldsymbol{\omega}_B$ are the frequencies at system buses; $\mathbf{B}_{BB}$ is the network susceptance matrix, i.e., the imaginary part of the standard network admittance matrix; $\mathbf{B}_{BG}$ is the susceptance matrices obtained using the internal impedances of the synchronous machines; and $\mathbf{B}_{G0}$ is a diagonal matrix that accounts for the internal susceptances of the synchronous machines at generator buses.

With respect to the COI expression given in (1), (2) has the advantage to provide *local* frequency estimations at every bus of the grid. Such values depend only on synchronous machine rotor speeds, which are continuous, and system topology, i.e., the admittance matrix of the grid.

III. Frequency Control of VSC-based Devices

A. Wind Turbines

Among all frequency control techniques of wind turbines that have been proposed in the literature, the most common approach is to vary the output of the Maximum Power Point Tracking (MPPT) based on the deviation of the measured frequency (droop control) or Rate of Change of Frequency (ROCOF) [11]–[13]. These controllers are briefly described below.

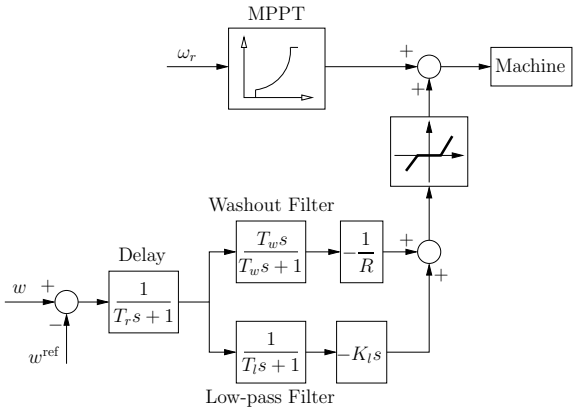

Fig. 2: Scheme of the droop and ROCOF controllers coupled to the MPPT.

Figure 2 shows the primary controller considered in this paper [14]. It includes:

- A ROCOF controller, which is composed of a low-pass filter, with time constant T_l, and the time derivative of frequency with negative gain $-K_l$. The low-pass filter eliminates both noise and numerical errors due to the numerical derivative of the frequency error.
- A droop control, which is composed of a washout-filter with time constant T_w, followed by a negative droop gain.

The ROCOF and droop controller are complementary. The ROCOF control, in fact, is faster and has its main effect in the very first instants after a contingency. The droop control, on the other hand, is slower and mitigates the frequency deviation. The output of the frequency controller is then added to the output of the MPPT.

B. Energy Storage Systems

A general scheme of a VSC-based ESS connected to a power system is depicted in Fig. 3. In this configuration, the VSC device provides reactive power support by regulating the ac voltage at the Point of Common Coupling (PCC) with the grid, whereas the storage device provides active power support. The models of the VSC and storage devices, as well as their controllers, are based on a thorough selection of well-assessed models for transient and frequency stability analysis [15].

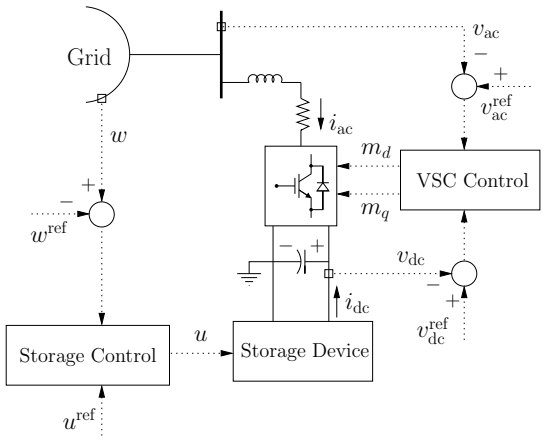

Fig. 3: Scheme of the ESS connected to a grid.

The input signal of the storage control is the error between a given frequency signal w, and a reference value (w^{ref}). The controller includes a dead-band and low-pass filter blocks. The aim of these blocks is to filter small, high-frequency perturbations in the frequency signal such as noises, reducing the number of operations of the storage device [16].

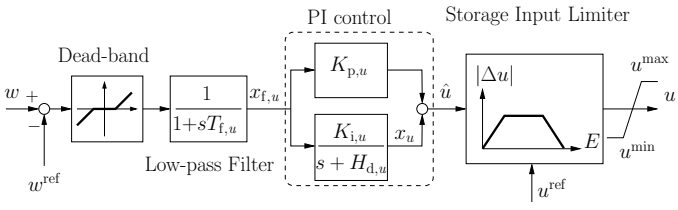

Fig. 4: Storage control scheme.

The controller shown in Fig. 4 also includes a Storage Input Limiter (SIL) block [17]. The aim of the SIL is to minimize the impact of energy saturation of the storage device on the transients of the ESS, and thus on those of the grid. The SIL regulates the input variable of the storage device, u, according to the actual value of the stored energy, E.

IV. Case Study

The case study is based on the well-known WSCC 9-bus, 3-machine test system. This network is composed of three synchronous machines, loads and transformers, and six transmission lines. The system also includes primary frequency and voltage regulation, i.e., Turbine Governors (TGs) and Automatic Voltage Regulators (AVRs), as well as secondary frequency regulation, i.e., an Automatic Generation Control (AGC). The scheme of the WSCC 9-bus system is shown in Fig. 5 and static and dynamic data can be found in [18].

The aim of this section is to compare the performance of the primary frequency control provided by an ESS and a WECS in Subsections IV-A and IV-B, respectively, when their input signal is provided by a PLL or by the frequency estimation approaches based on the COI and the FD.

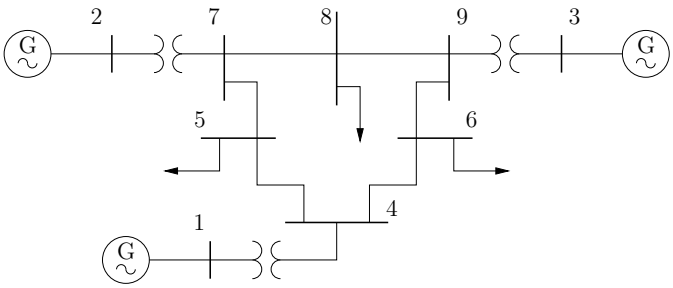

Fig. 5: Scheme of the WSCC 9-bus test system.

In order to provide a realistic evaluation of the accuracy and performance of the PLL and other different frequency estimation techniques, noise modeled as Ornstein-Uhlenbeck's process with Gaussian distribution is applied to the magnitudes and angles of all bus voltage phasors of the system. The interested reader can find in [19] a detailed description of the modeling and implementation of stochastic processes applied to bus voltage phasors.

A. WSCC Test System with an ESS

In this scenario, an ESS is installed and connected to bus 8. The storage technology considered is a Superconducting Magnetic Energy Storage (SMES) system [20]. The dc current flowing through the SMES, which can be stored for long periods due to its low internal losses, can be delivered to the grid in few milliseconds, and vice versa. The features of SMES systems make them suitable to reduce the impact of fast transients, e.g., faults and loss of lines, and to flatten the active power supplied by distributed energy sources such as wind power plants.

A three-phase fault is simulated at bus 7 at $t = 1$ s. The fault is cleared after 100 ms by opening the line connecting buses 7 and 5. The system load is increased by 25% with respect to base loading conditions. The SMES installed can provide 40 MW of peak power. For space limitation, the effects of hard limits of current controllers and energy stored in the SMES are not taken into account. The values of the parameters of the SMES controller depicted in Fig. 4 are listed in Table I.

TABLE I: Values of the parameters of the SMES controller.

Parameter	Value	Unit
$T_{\mathrm{f},u}$	0.1	s
$K_{\mathrm{p},u}$	13.0	–
$K_{\mathrm{i},u}$	20.0	–
$H_{\mathrm{d},u}$	1.0	–

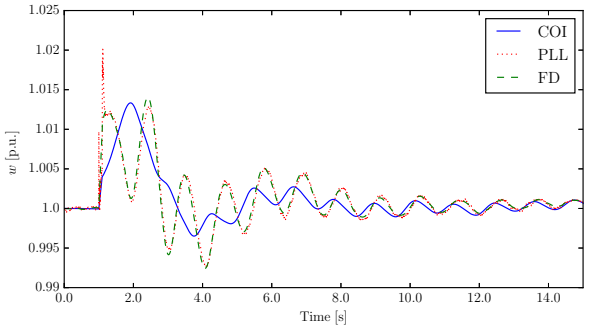

Fig. 6: Input frequency signal of the SMES active power control estimated by different approaches.

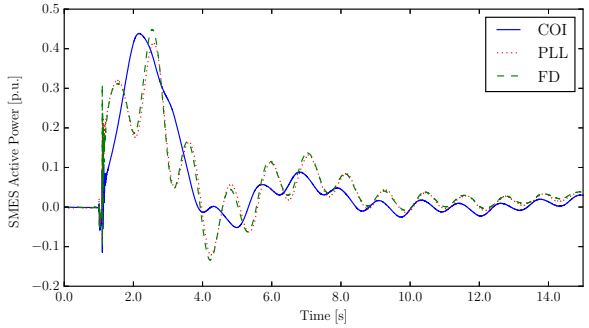

Fig. 7: Active power supplied/consumed by the SMES.

Figure 6 shows the input signal w of the SMES active power controller estimated using the three different approaches, namely frequency of the COI and of bus 8 estimated with both the FD and an ideal PLL (i.e., no delay, $\tau = 0$). It can be observed that there is a significant difference between the effect of local (PLL and FD) and global (COI) frequency signals on the controller. Such a difference leads to different responses of the SMES, as shown in Fig. 7, where positive power represents energy being stored, and vice versa.

The impact of SMES responses on the rest of the system is represented in Fig. 8, where the rotor angle (Fig. 8(a)) and speed (Fig. 8(b)) of the synchronous machine at bus 3 are depicted. While the machine oscillations after the fault are poorly damped when the frequency is estimated by the COI, these oscillations vanish faster in the case of the PLL and the FD. Moreover, the amplitude of the first swing of the rotor angle is higher when considering the COI, increasing the risk of loss of synchronism of the machine. In fact, the critical clearing times of the fault is 113 ms when the signal w is estimated by the COI, and 127 ms for the PLL and the FD cases.

It is worth noticing that, despite the PLL and the FD are

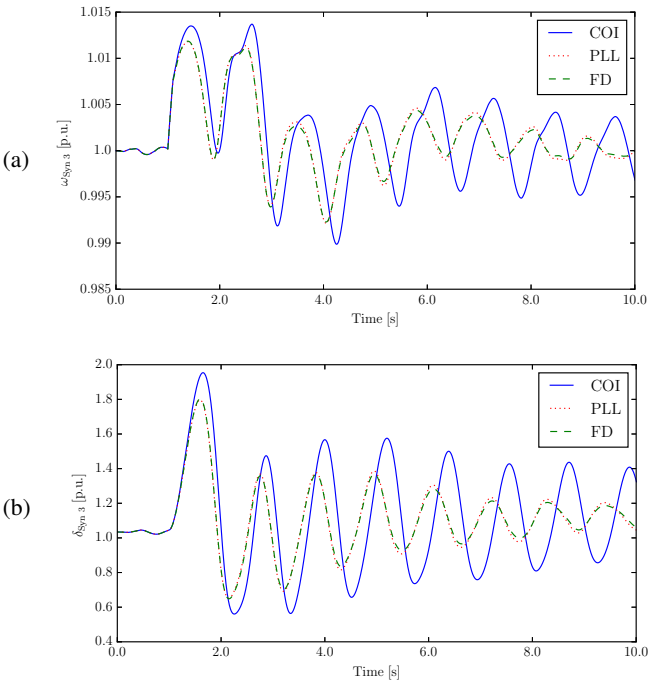

Fig. 8: Response of the synchronous machine at bus 3 following a three-phase fault: (a) rotor angle; and (b) rotor speed.

conceptually completely different, they show a fairly similar estimation of local frequencies. From Fig. 6, the main difference between the two techniques is the spike present in the PLL signal during the first transients after the fault occurrence, and a higher sensitivity to the noise of the bus voltage magnitudes and angles. However, as seen in Figs. 7 and 8, both the spike and the noise are filtered by the storage control of Fig. 3, and hence the similar performance of the SMES for the two estimation techniques during and after the transient.

The effect of a non-null delay τ in the input signal θ of the PLL and for the same fault simulated above is shown in Fig. 9. Two time delays are considered, namely, 20 ms and 100 ms. As expected, the delay affects the quality of the signal obtained by the PLL. Longer delays imply bigger spikes during the transient, and longer settling times, which lead to poorer performance of the SMES and of thus the overall system. Therefore, it is important to minimize the delays of the frequency estimation process.

B. WSCC Test System with a WECS

In this scenario, the synchronous machine at bus 3 has been replaced with a wind power plant of the same capacity, composed of 50 variable-speed wind turbines modeled with a 5^{th}-order Doubly-Fed Induction Generation (DFIG) model [21]. The stochastic process applied to the wind follows a Weibull distribution [22]. The contingency is the outage of the line connecting buses 5 and 7 at $t = 30$ s. The values of the parameters of the WECS are based on [23], whereas the values of the parameters of the controller depicted in Fig. 2 are provided in Table II.

(a)

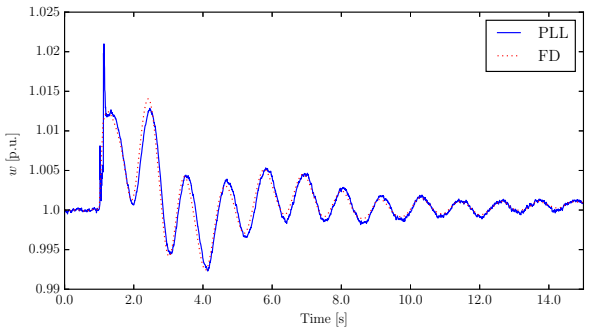

(b)

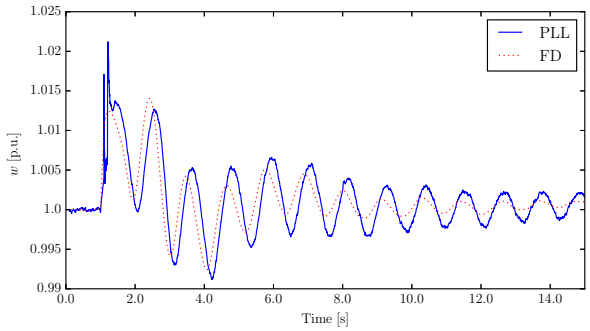

Fig. 9: Input local frequency signal of the SMES active power control when the PLL includes a delay: (a) 20 ms delay; and (b) 100 ms delay.

TABLE II: Values of the parameters of the WECS controller.

Parameter	Value	Unit
$T_{r,u}$	0.5	s
$T_{w,u}$	1000.0	s
$T_{l,u}$	4.0	s
R	0.05	–
K_l	80.0	–

The input signals of the wind plant controller and the subsequent active power outputs are represented in Figs. 10 and 11, respectively, for the different frequency estimation approaches. As opposed to the case with the SMES in the previous subsection, in this scenario the difference between the signals is relatively small, leading to similar active powers supplied by the wind power plant.

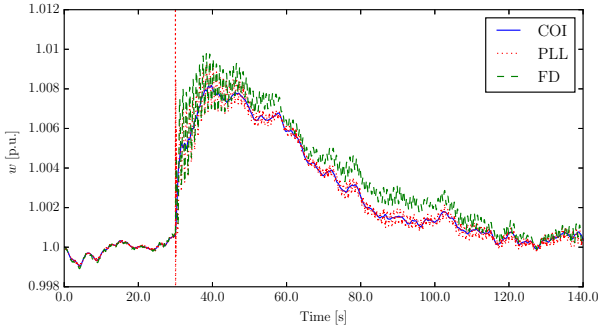

Fig. 10: Input frequency signal of the wind power plant control estimated by different approaches.

The response of the frequency of the COI is represented in Fig. 12 for each of the frequency estimation approaches, and compared with that without the controller of the wind power plant. The inclusion of such controller reduces the frequency peak caused by the loss of the load by about 30-40%, being the lowest when the FD formula is used as input signal of the controller. Note that the frequency spikes that can be observed in Fig. 10 when using the PLL, which vary in the range of $[0.99, 1.02]$ pu, are filtered by the WECS controller.

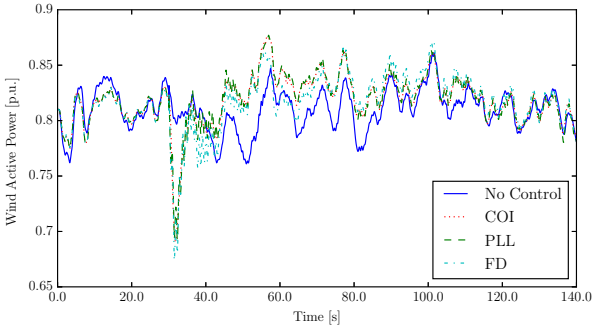

Fig. 11: Active power supplied by the wind power plant.

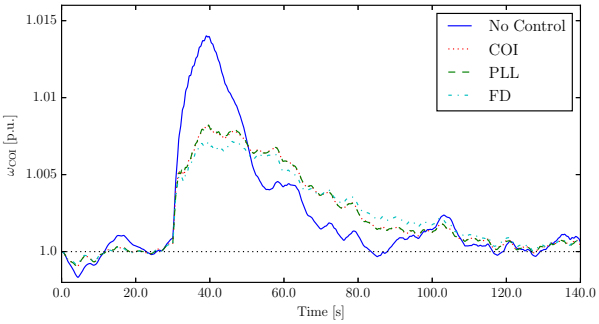

Fig. 12: Frequency of the COI.

Finally, to study the sensitivity of the three frequency estimation techniques to fast system dynamics, the flux dynamics of the DFIGs are included in the model. Results are shown in Fig. 13. It can be seen that, while the behavior of the COI and the FD is similar to the one when no flux dynamics were included, the PLL now shows fast varying, poorly damped oscillations that leads to frequency fluctuations in the range of $[0.99, 1.023]$ pu.

These results suggest that fast dynamics can negatively affect the response of controllers based on local frequency measures and that an appropriate filtering should be implemented if PLL devices are to be utilized. On the other hand, filtering should not introduce a delay in the frequency measure to prevent the deterioration in the dynamic response observed in Fig. 9.

V. Conclusions

The paper discusses the impact of modeling PLL devices for the primary frequency regulation of wind turbines and energy storage systems. The proposed model of the PLL is then compared with the frequency estimation provided by the center of inertia and the frequency divider formula. The latter approach, which was previously proposed by the authors, appears to provide the *ideal* value of the local frequency at buses and can thus be utilized as a reference for testing the quality of the frequency estimated by the PLLs.

Simulation results indicate that a standard synchronous reference frame model of the PLL works reasonably well compared to the FD. Noise and numerical spikes do not appear to significantly deteriorate the quality of the control, provided that wind turbine and ESS devices include a proper low pass filter within their primary frequency controllers. Fast dyanmics of fluxes, however, can deteriorate the dynamic response of PLL-based frequency controllers.

On the other hand, the COI signal appears inadequate to simulate the behavior of primary frequency controllers, although its average nature often leads to an overall smoother frequency response. This consideration could be further developed in the future considering coordinated area controllers sharing an average value of the frequency signal rather than utilizing a local one.

Acknowledgments

This material is based upon works supported by the European Commission Ireland, by funding Á. Ortega and F. Milano, under Grant No. 727481, RE-SERVE, H2020-LCE-2016-RES-CCS-RIA. The authors wish to acknowledge the useful discussions with the RE-SERVE partners, Dr. Catalin Chimirel (TransElectrica) and Prof. Lucian Toma (UPB). F. Milano is also a beneficiary of financial support from the EC Marie Skłodowska-Curie Career Integration Grant No. PCIG14-GA-2013-630811.

References

[1] O. Anaya-Lara, F. Hughes, N. Jenkins, and G. Strbac, "Contribution of DFIG-based Wind Farms to Power System Short-term Frequency Regulation," *IEE Procs. on Generation, Transmission and Distribution*, vol. 153, no. 2, pp. 164–170, March 2006.

[2] P. Moutis, A. Vassilakis, A. Sampani, and N. Hatziargyriou, "DC Switch Driven Active Power Output Control of Photovoltaic Inverters for the Provision of Frequency Regulation," *IEEE Trans. on Sustainable Energy*, vol. 6, no. 4, pp. 1485–1493, Oct 2015.

[3] Á. Ortega and F. Milano, "Modeling, Simulation and Comparison of Control Techniques for Energy Storage Systems," *IEEE Trans. on Power Systems*, 2016, (in press).

[4] A. Nicastri and A. Nagliero, "Comparison and evaluation of the pll techniques for the design of the grid-connected inverter systems," in *2010 IEEE International Symposium on Industrial Electronics*, July 2010, pp. 3865–3870.

[5] Á. Ortega and F. Milano, "Comparison of bus frequency estimators for power system transient stability analysis," in *POWERCON*, Wollongong, Australia, Sept. 2016.

[6] M. Pavella, D. Ernst, and D. Ruiz-Vega, *Transient Stability of Power Systems – A Unified approach to Assessment and Control*. Boston: Kluwer Academic Publishers, 2000.

[7] F. Milano and Á. Ortega, "Frequency Divider," *IEEE Trans. on Power Systems*, 2016, (in press).

[8] IEEE Task Force on Load Representation for Dynamic Performance, "Load Representation for Dynamic Performance Analysis [of Power Systems]," *IEEE Trans. on Power Systems*, vol. 8, no. 2, pp. 472–482, May 1993.

[9] H. Karimi, M. Karimi-Ghartemani, and M. R. Iravani, "Estimation of frequency and its rate of change for applications in power systems," *IEEE Trans. on Power Delivery*, vol. 19, no. 2, pp. 472–480, April 2004.

[10] F. Blaabjerg, R. Teodorescu, M. Liserre, and A. V. Timbus, "Overview of control and grid synchronization for distributed power generation systems," *IEEE Trans. on Industrial Electronics*, vol. 53, no. 5, pp. 1398–1409, Oct 2006.

[11] G. Ramtharan, J. B. Ekanayake, and N. Jenkins, "Frequency support from doubly fed induction generator wind turbines," *IET Renewable Power Generation*, vol. 1, no. 1, pp. 3–9, March 2007.

[12] J. Ekanayake and N. Jenkins, "Comparison of the Response of Doubly Fed and Fixed-Speed Induction Generator Wind Turbines to Changes in Network Frequency," *IEEE Trans. on Energy Conversion*, vol. 19, no. 4, pp. 800–802, Dec. 2004.

[13] J. Morren, S. W. H. de Haan, W. L. Kling, and J. A. Ferreira, "Wind turbines emulating inertia and supporting primary frequency control," *IEEE Trans. on Power Systems*, vol. 21, no. 1, pp. 433–434, Feb 2006.

[14] J. Cerqueira, F. Bruzzone, C. Castro, S. Massucco, and F. Milano, "Comparison of the dynamic response of wind turbine primary frequency controllers constraints," in *IEEE PES General Meeting*, July 2017.

[15] Á. Ortega and F. Milano, "Generalized Model of VSC-Based Energy Storage Systems for Transient Stability Analysis," *IEEE Trans. on Power Systems*, vol. 31, no. 5, pp. 3369–3380, Sept 2016.

[16] F. Milano and R. Zárate-Miñano, "Study of the Interaction between Wind Power Plants and SMES Systems," in *12th Wind Integration Workshop*, London, UK, Oct. 2013.

[17] Á. Ortega and F. Milano, "Design of a Control Limiter to Improve the Dynamic Response of Energy Storage Systems," in *Power Engineering Society General Meeting, IEEE*, Denver, Colorado, USA, July 2015.

[18] P. M. Anderson and A. A. Fouad, *Power System Control and Stability*, 2nd ed. Wiley-IEEE Press, 2003.

[19] F. Milano and R. Zárate-Miñano, "A systematic method to model power systems as stochastic differential algebraic equations," *IEEE Trans. on Power Systems*, vol. 28, no. 4, pp. 4537–4544, Nov 2013.

[20] IEEE Task Force on Benchmark Models for Digital Simulation of FACTS and Custom-Power Controllers, T&D Committee, "Detailed modeling of superconducting magnetic energy storage (SMES) system," *IEEE Trans. on Power Delivery*, vol. 21, no. 2, pp. 699–710, Apr. 2006.

[21] J. G. Slootweg, H. Polinder, and W. L. Kling, "Dynamic modelling of a wind turbine with doubly fed induction generator," in *IEEE PES Summer Meeting*, vol. 1, July 2001, pp. 644–649 vol.1.

[22] F. Milano, *Power System Modelling and Scripting*. London: Springer, 2010.

[23] M. Singh and S. Santoso, "Dynamic models for wind turbines and wind power plants," NREL, Tech. Rep., Oct 2011. [Online]. Available: http://www.osti.gov/scitech/servlets/purl/1028524

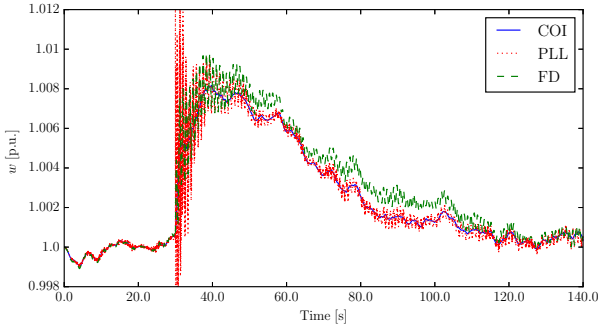

Fig. 13: Input frequency signal of the wind power plant control estimated by different approaches with inclusion of DFIG flux dynamics.